Cell

Absence of CNTNAP2 Leads to Epilepsy, Neuronal Migration Abnormalities, and Core Autism-Related Deficits

Olga Peñagarikano,[1,2,3] Brett S. Abrahams,[2,3,6] Edward I. Herman,[2,7] Kellen D. Winden,[1,2] Amos Gdalyahu,[4] Hongmei Dong,[2] Lisa I. Sonnenblick,[2] Robin Gruver,[4] Joel Almajano,[2] Anatol Bragin,[2] Peyman Golshani,[2] Joshua T. Trachtenberg,[4] Elior Peles,[5] and Daniel H. Geschwind[1,2,3,*]

[1]Program in Neurogenetics, Department of Neurology, David Geffen School of Medicine
[2]Department of Neurology, David Geffen School of Medicine
[3]Center for Autism Research and Treatment and Center for Neurobehavioral Genetics, Semel Institute for Neuroscience and Human Behavior
[4]Department of Neurobiology, David Geffen School of Medicine
University of California, Los Angeles, CA 90095, USA
[5]Department of Molecular Cell Biology, The Weizmann Institute of Science, Rehovot 76100, Israel
[6]Present address: Departments of Genetics and Neuroscience, Price Center for Genetic and Translational Medicine, Albert Einstein College of Medicine, Bronx, NY 10461, USA
[7]Present address: Yale MSTP Program, Yale School of Medicine, New Haven, CT 06511, USA
*Correspondence: dhg@ucla.edu
DOI 10.1016/j.cell.2011.08.040

SUMMARY

Although many genes predisposing to autism spectrum disorders (ASD) have been identified, the biological mechanism(s) remain unclear. Mouse models based on human disease-causing mutations provide the potential for understanding gene function and novel treatment development. Here, we characterize a mouse knockout of the *Cntnap2* gene, which is strongly associated with ASD and allied neurodevelopmental disorders. *Cntnap2*$^{-/-}$ mice show deficits in the three core ASD behavioral domains, as well as hyperactivity and epileptic seizures, as have been reported in humans with *CNTNAP2* mutations. Neuropathological and physiological analyses of these mice before the onset of seizures reveal neuronal migration abnormalities, reduced number of interneurons, and abnormal neuronal network activity. In addition, treatment with the FDA-approved drug risperidone ameliorates the targeted repetitive behaviors in the mutant mice. These data demonstrate a functional role for *CNTNAP2* in brain development and provide a new tool for mechanistic and therapeutic research in ASD.

INTRODUCTION

Autism spectrum disorders (ASD) form a heterogeneous neurodevelopmental syndrome characterized by deficits in language development, social interactions, and repetitive behavior/restricted interests (APA, 2000). Although not necessary for diagnosis, a number of other neurological or behavioral abnormalities are frequently associated with ASD, including hyperactivity, epilepsy, and sensory processing abnormalities (Geschwind, 2009).

Research into the genetic basis for ASD has identified many genes, including common and rare variants (Sebat et al., 2007; Glessner et al., 2009; Weiss et al., 2009). Association, linkage, gene expression, and imaging data support the role of both common and rare variants of *contactin associated protein-like 2* (*CNTNAP2*) in ASD. Originally, a recessive nonsense mutation in *CNTNAP2* was shown to cause a syndromic form of ASD, cortical dysplasia-focal epilepsy syndrome (CDFE), a rare disorder resulting in epileptic seizures, language regression, intellectual disability, hyperactivity, and, in nearly two-thirds of the patients, autism (Strauss et al., 2006). Several reports have since linked this gene to an increased risk of autism or autism-related endophenotypes (Alarcón et al., 2008; Arking et al., 2008; Bakkaloglu et al., 2008; Vernes et al., 2008). Recently, we have shown that the same *CNTNAP2* variant that increases risk for the language endophenotype in autism leads to abnormal functional brain connectivity in human subjects (Scott-Van Zeeland et al., 2010), consistent with emerging theories of ASD pathophysiology based on altered neuronal synchrony and disconnection (Belmonte et al., 2004).

Cntnap2 (also known as *Caspr2*) encodes a neuronal transmembrane protein member of the neurexin superfamily involved in neuron-glia interactions and clustering of K^+ channels in myelinated axons (Poliak et al., 1999; 2003). However, the fact that the gene is expressed embryonically (Poliak et al., 1999; Abrahams et al., 2007; Alarcón et al., 2008) and myelination takes place postnatally, together with the increasing number of reports that link the gene to ASD, suggest an additional role for *CNTNAP2* in early brain development. This is supported by the imaging and pathology data in patients with CDFE, in whom nearly half manifest presumed neuronal migration abnormalities on MRI, confirmed by histological analysis of brain tissue resected from patients who underwent surgery for epilepsy (Strauss et al., 2006).

The generation of valid animal models is critical for understanding the pathophysiology of ASD and to assess the potential of proposed treatments, as well as developing new, effective interventions. Ideally, mouse models should be based on a known genetic cause of the disease (construct validity), reflect key aspects of the human symptoms (face validity), and respond to treatments that are effective in the human disease (predictive validity) (Chadman et al., 2009; Nestler and Hyman, 2010). Here, we demonstrate that the *Cntnap2* knockout mouse exhibits striking parallels to the major neuropathological features in CDFE and the core features of ASD. We observe defects in the migration of cortical projection neurons and a reduction in the number of GABAergic interneurons, as well as accompanying neurophysiological alterations. These data show that CNTNAP2 is involved in the development of cortical circuits and further support alterations in brain synchrony or connectivity in ASD pathophysiology. In addition, treating *Cntnap2*$^{-/-}$ mice with risperidone rescues the repetitive behavior, but not the social deficits, a dissociation parallel to what is seen in human patients. These data demonstrate the validity of the *Cntnap2* KO as a mouse model for ASD and provide initial insight into the underlying mechanisms by which CNTNAP2 affects brain development and function.

RESULTS

Expression of *Cntnap2* in Mouse Brain

Mutant mice lacking the *Cntnap2* gene (*Caspr2* null mice) were generated by Dr. Elior Peles (Poliak et al., 2003). We backcrossed the original ICR outbred strain onto the C57BL/6J background for 10–12 generations. *Cntnap2*$^{-/-}$ mice on the C57BL/6J background had a normal appearance; no differences in weight or growth rate were observed when compared with WT littermates. In WT brain, expression of CNTNAP2 was first detected by western blot around embryonic day 14 (E14). As expected, CNTNAP2 was completely absent in the brain of homozygous mutant animals (Figure S1A available online). In situ hybridization demonstrated *Cntnap2* expression in multiple adult brain regions, primarily cerebral cortex, hippocampus, striatum, olfactory tract, and cerebellar cortex (Figure S1B). Embryonic expression was also broad, including the ventricular proliferative zones of the developing cortex and ganglionic eminences (where excitatory projection neurons and inhibitory interneurons arise, respectively) overlapping with regions containing migrating neurons and postmigratory cells, indicating a possible role in neuron development and/or migration (Figure S1C).

Cntnap2$^{-/-}$ Mice Exhibit Epileptic Seizures and Abnormal Electroencephalogram Pattern

One of the major phenotypes of CDFE syndrome is the presence of epileptic seizures, which is associated with dense hippocampal astroglyosis (Strauss et al., 2006). In *Cntnap2*$^{-/-}$ mice, spontaneous seizures were commonly observed in animals older than 6 months of age. Seizures were consistently induced by mild stressors during routine handling (Movie S1). A behavioral study of the frequency and severity of the seizures (Racine, 1972) is presented in Table S1. Histological analysis of the hippocampal formation in these animals did not show any gross structural abnormalities, although a reduction in parvalbumin-positive interneurons was found (see below and Figure S3C). Reactive astrocytosis as indicated by an enhanced expression of glial fibrillary acidic protein (GFAP) was observed throughout the hippocampus of mutant mice after the onset of seizures. Reactive astrocytosis was especially dense in the hilus but was not accompanied by neuronal loss in this structure as indicated by neuronal nuclei (NeuN) staining (Figure 1A). Electroencephalogram (EEG) recordings from freely moving mutant animals implanted with cortical electrodes at 8 months of age showed generalized interictal spike discharges during slow-wave sleep, whereas no electrical abnormalities were found in the EEG of mutant mice at times before the onset of seizures (Figure 1B). To avoid any confounding effect due to the presence of epileptic seizures, the following neuropathological, physiological, and behavioral characterization of *Cntnap2* mutants was performed at an age before the onset of seizures.

Cntnap2$^{-/-}$ Mice Show Neuronal Migration Abnormalities

We performed detailed histological analyses of *Cntnap2* KO brain and found no gross morphological changes in the brain structure of mutant animals by conventional staining techniques (cresyl violet staining), consistent with previous reports (Poliak et al., 2003). NeuN immunohistochemistry (IHC) revealed the presence of ectopic neurons in the corpus callosum of mutant mice at postnatal day 14 (P14), after neuronal migration is completed, which persisted through adulthood (Figure 2A). Interestingly, ectopic neurons of unknown origin in white matter were also reported in CDFE syndrome patients (Strauss et al., 2006).

Patients with CDFE syndrome also show neuronal migration abnormalities, such as abnormal arrangements of neurons in clusters or migratory rows in the deep layers of cortex (Strauss et al., 2006). We assessed laminar positioning of cortical projection neurons in WT and *Cntnap2* KO mice with antibodies against CUX1, a marker for upper-cortical layers, and FOXP2, a marker for deep cortical layers (Molyneaux et al., 2007). *Cntnap2*$^{-/-}$ mice show significantly higher numbers of CUX1+ cells in deep cortical layers (V and VI; Figure 2B). In contrast, deeper-layer FOXP2+ cells show the same pattern in both genotypes (Figure S2).

We performed BrdU neuron birthdating at E16.5, after the birth of layer V neurons (Angevine and Sidman, 1961) to confirm that the CUX1+ ectopic neurons observed in deep cortical layers were being born concomitant with superficial cell identity and their presence was not due to changes in cell fate. Sections of E16.5-labeled animals were analyzed at P7, when cortical lamination is essentially complete. As shown in Figure 2C, the distribution of BrdU+ cells is significantly different between WT and KO littermates, the latter showing a shortage of cells in upper-cortical layers that are redistributed to lower cortical layers. These data indicate that CNTNAP2 is necessary for the normal migration of cortical projection neurons.

Reduced Number of Interneurons in *Cntnap2*$^{-/-}$ Mice

Since the identification of CNTNAP2 (CASPR2) in 1999 (Poliak et al., 1999), its expression has been reported mainly in

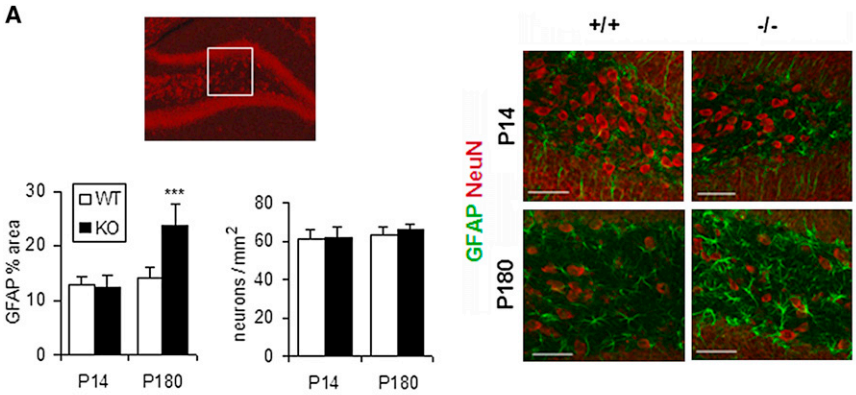

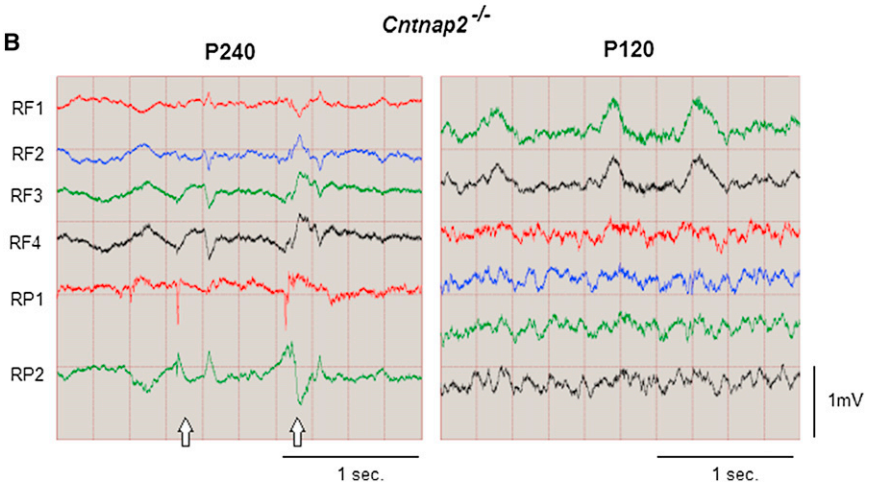

Figure 1. *Cntnap2*$^{-/-}$ Mice Show Epileptic Seizures and Abnormal EEG Pattern

(A) Presence of reactive astrocytes in the hippocampal hilus (inset) of P180, but not P14, mutant mice without significant changes in neuronal density. GFAP, glial fibrillary acidic protein; NeuN, neuronal nuclei. Scale bar, 50 μm. GFAP quantification is shown as percentage of area occupied by reactive astrocytes. n = 4 mice/genotype for each age. Data are presented as mean ± SEM. ***$p < 0.001$.

(B) EEG recording from mutant mice shows abnormal spike discharges (arrows) after seizure onset. n = 3 mice for each age. RF, right frontal; RP, right parietal.

See also Table S1, Movie S1 and Figure S3C.

excitatory pyramidal cells at the axon initial segment (Inda et al., 2006) and myelinated axons (Poliak et al., 2003, Horresh et al., 2008). The embryonic expression of *Cntnap2* in the ganglionic eminence, where GABAergic interneurons arise, led us to analyze the expression of CNTNAP2 in interneurons. We analyzed available microarray data from single glutamatergic and GABAergic neuronal populations isolated from adult mice (Sugino et al., 2006) using weighted gene coexpression network analysis (WGCNA) (Zhang and Horvath, 2005). WGCNA groups functionally related genes into modules based on expression in a way such that genes showing similar expression patterns across samples are grouped together. Modules are likely to represent biological pathways in a way that they are usually coregulated or interact (Oldham et al., 2008). Interestingly, we found that *Cntnap2* is part of a module with enriched expression in inhibitory relative to excitatory neurons (Figure S3A and Table S2). In addition, three of the most highly connected genes within the module, which are indicative of module function, are *Gad1*, *Gad2*, and *Slc32a1* (*VGAT*), genes that are known to be necessary for GABAergic transmission (Figure 3A), suggesting the possibility of CNTNAP2 involvement in interneuron functioning.

Because the potential relationship of CNTNAP2 to GABAergic interneuron function had not been previously explored and interneuron dysfunction has been associated with autism and epilepsy (Levitt et al., 2004), we analyzed the number and distribution of interneurons in *Cntnap2*$^{-/-}$ mice. GAD1 immunostaining showed that *Cntnap2*$^{-/-}$ mice have a reduced number of GABAergic interneurons in all laminae (Figure 3B). To test whether the reduction in interneurons was subtype specific, we analyzed the number and distribution of the largely nonoverlapping subgroups of interneurons in rodents: parvalbumin (PVALB), calretinin (CALB2) and neuropeptide Y (NPY) (Wonders and Anderson, 2006). We observed that PVALB+ interneurons were the most affected (Figure 3C). Because striatal interneurons are also born in the ganglionic eminence (Marín et al., 2001), we next examined the number of interneurons in the striatum. We observed a reduction of striatal GABAergic interneurons in mutants (Figure 3D) without a change in cholinergic interneurons (Figure S3B). PVALB+ interneurons were also reduced in the hippocampus (Figure S3C). Together, these data indicate a role for CNTNAP2 in GABAergic interneuron development.

Cntnap2$^{-/-}$ Mice Show Reduced Cortical Neuronal Synchrony

The abnormal positioning and migration of excitatory principal neurons and reduction in inhibitory interneurons suggested that neuronal network activity might be abnormal. This was particularly important, as GABAergic interneurons are recognized as playing a crucial role in the precise timing of neuronal activity (Sohal et al., 2009) and there is increasing evidence of abnormal neural synchrony as a pathophysiological mechanism in ASD (Uhlhaas and Singer, 2006; Belmonte et al., 2004). In vivo two-photon calcium imaging of layer II/III neurons from somatosensory cortex (Figure 4A) indicated that the neuronal firing pattern of *Cntnap2*$^{-/-}$ mice was highly asynchronous relative to WT mice (Figure 4B). The mean correlation coefficient of the firing timing between all cell pairs of neurons over the distance range analyzed was significantly lower in mutant mice

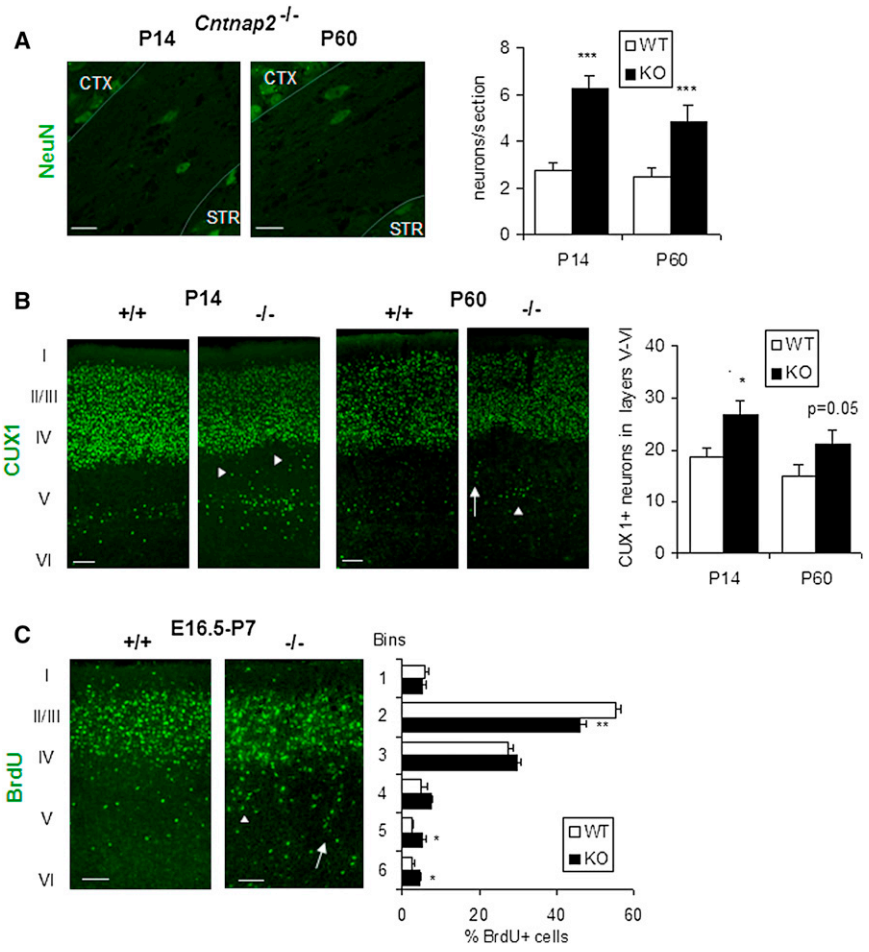

Figure 2. *Cntnap2*$^{-/-}$ Mice Show Neuronal Migration Abnormalities

(A) Presence of ectopic neurons in the corpus callosum of *Cntnap2*$^{-/-}$ mice. NeuN, neuronal nuclei; CTX, cortex; STR, striatum. Scale bar, 20 μm.

(B) Expression of *Cux1*, a marker for upper-layer projection neurons, in somatosensory cortex of WT and *Cntnap2*$^{-/-}$ mice. Note the abnormal distribution of CUX1-positive cells in groups (arrowheads) and rows (arrow) in deep cortical layers of mutant mice. Scale bar, 50 μm.

(C) Neuronal birthdating analysis. BrdU injected at E16.5 was immunostained at P7. Note abnormal distribution of neurons in groups (arrowheads) and rows (arrow) in deep cortical layers of mutant animals. Scale bar, 50 μm.

Data are presented as mean ± SEM. *$p < 0.05$, **$p < 0.01$, ***$p < 0.001$. n = 3 mice/genotype for each age. See also Figure S2.

(Figure 4C). In addition, neither the average firing amplitude (Figure 4D) nor the average firing rate (Figure 4E) changed significantly between genotypes, suggesting that the asynchronous firing observed in mutant animals is likely due to a network dysfunction rather than to abnormalities in neuronal activity or conduction per se. This is consistent with previous data that show no alterations in peripheral and central nerve conductance in *Cntnap2*$^{-/-}$ mice (Poliak et al., 2003).

Behavioral Characterization of *Cntnap2*$^{-/-}$ Mice

Because the diagnostic criteria in ASD are currently based on behavioral symptoms rather than molecular or neuroanatomical indicators, we performed a complete battery of behavioral tests to examine the potential effect of the absence of CNTNAP2 on behavior. A summary of the tests performed relevant to each behavioral domain related to ASD (Silverman et al., 2010), and the results obtained are presented in Table S3.

Cntnap2$^{-/-}$ mice displayed significantly greater locomotor activity than their WT littermates in the open field test (Figures S4A and S4B). This increased activity was also noted when testing for motor coordination and balance with the rotorod, as mutant mice performed significantly better than WT (Figure S4C). Interestingly, several animal models of autism (Kwon et al., 2006; Nakatani et al., 2009) and hyperactivity (Gerlai et al., 2000; Vitali and Clarke, 2004) have been reported to perform better in the rotorod test.

To assess anxiety-related responses, we performed the light-dark exploration test and observed no significant differences between genotypes (Figure S4D). Potential sensory deficits were assessed with the hot plate test. As shown (Figure S4E), *Cntnap2*$^{-/-}$ mice demonstrated hyperreactivity to thermal sensory stimuli. To further characterize this sensory deficit, we measured the acoustic startle response (Figure S4F) and the degree of prepulse inhibition (Figure S4G) and found no significant differences between genotypes. In addition, olfaction analysis did not show any deficit in mutant mice but, rather, appeared to perform better than WT mice in the buried food test (Figure S4H).

Cntnap2$^{-/-}$ Mice Show Stereotypic Motor Movements and Behavioral Inflexibility

Spatial learning and memory were evaluated in the Morris water maze (MWM). Both WT and mutant mice showed similar learning curves, represented as time to locate the platform in the training phase of the test (Figure 5A). Probe trials were performed the day after the last training trial, and an active search for the platform was evaluated. As expected from their learning curves, WT and KO animals performed similarly in the probe test (Figures 5B and 5C).

To assess behavioral flexibility and perseveration, we first performed a classic reversal task using the MWM. We found that *Cntnap2*$^{-/-}$ mice showed impairment in learning the new location of the platform (Figure 5D) and performed poorly in the probe test (Figures 5E and 5F). To study perseveration in more detail, we performed the spontaneous alternation T maze test. As shown in Figure 5G, *Cntnap2*$^{-/-}$ mice showed significantly higher number of no alternations in a standard 10 trial test,

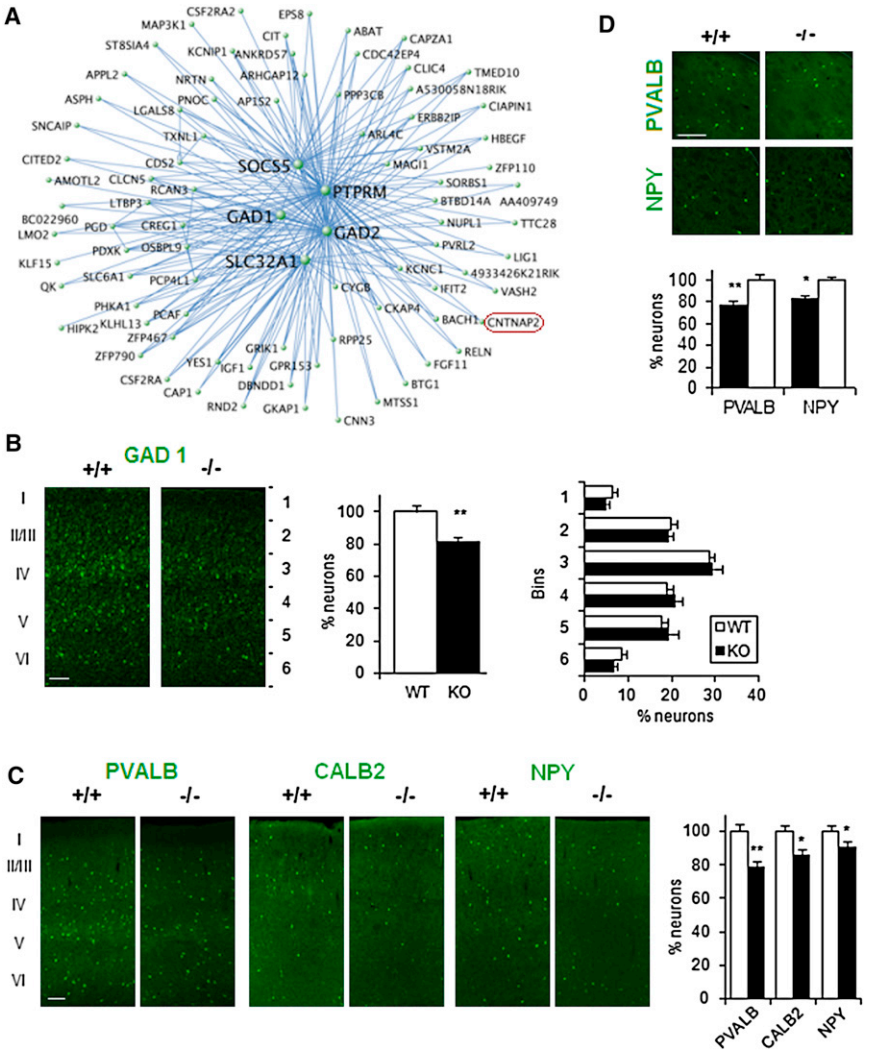

Figure 3. Reduced Number of GABAergic Interneurons in *Cntnap2*$^{-/-}$ Mice

(A) Network plot showing the top 300 connections within the *Cntnap2* module.

(B) Expression of *Gad1* at P14 shows a reduced number of GABAergic interneurons in somatosensory cortex of KO mice. Scale bar, 50 μm.

(C) Expression of the interneuron markers PVALB, CALB2, and NPY at P14. Scale bar, 50 μm.

(D) Expression of the GABAergic markers PVALB and NPY in striatum. Scale bar, 100 μm. Interneuron quantification is shown as percentage of WT.

*$p < 0.05$ and **$p < 0.01$. For (B)–(E), n = 4 mice/genotype. Data are presented as mean ± SEM. See also Table S2 and Figure S3.

confirming the perseveration observed in the reversal task on the MWM. In addition to perseveration, repetitive behavior also encompasses motor stereotypies, and both tend to co-occur in children with ASD. Consistent with our other observations, we found that *Cntnap2*$^{-/-}$ mice spent almost three times more time grooming themselves than their WT littermates (Figure 5H).

Cntnap2$^{-/-}$ Mice Show Communication and Social Behavior Abnormalities

Isolation-induced ultrasonic vocalizations (UsVs) are distress calls emitted by pups when separated from their mother, representing an infant-mother vocal communicative behavior that is thought to be relevant to ASD (Crawley, 2007; Silverman et al., 2010). We analyzed the pattern of UsV emission in WT and *Cntnap2*$^{-/-}$mice through development (P3, P6, P9, and P12; Scattoni et al., 2009) and found that *Cntnap2*$^{-/-}$ mice emitted a significantly lower number of ultrasonic calls than WT littermates at all ages (Figure 6A).

We next analyzed social behavior in pairs of unfamiliar mice at age P21 (juvenile play test). As shown in Figure 6B, *Cntnap2*$^{-/-}$ mice spent significantly less time interacting with each other and instead showed increased repetitive behaviors such as grooming and digging. We confirmed that the abnormal social behavior was not due to an olfaction defect (Table S3), as *Cntnap2* mutant mice actually perform significantly better than WT in the buried food olfaction test (Figure S4H). We also performed a three-chamber social interaction test in adults (Crawley, 2007). As expected for the highly social strain C57/B6J, WT mice showed a highly significant preference for the cup with a mouse, whereas KO mice did not show a significant preference (Figure 6C). Finally, we examined nest-building behavior, which is relevant to home-cage social behaviors and mediated by dopaminergic function in mice (Szczypka et al., 2001). *Cntnap2*$^{-/-}$ mice were also significantly impaired in this task (Deacon, 2006), scoring less than half of the WT criterion (Figure 6D).

The Atypical Antipsychotic Risperidone Rescues the Hyperactivity, Repetitive Behavior/Perseveration, and Nesting Deficits in *Cntnap2*$^{-/-}$ Mice

An important goal in developing mouse models of neuropsychiatric diseases is testing therapeutic treatments. Risperidone was the first drug approved by the United States Food and Drug Administration (FDA) for symptomatic treatment of ASD, alleviating hyperactivity, repetitive behavior, aggression, and self-injurious behavior (McDougle et al., 2000, 2008). *Cntnap2*$^{-/-}$ mice and their WT littermates were treated with risperidone or vehicle for 7–10 days and were tested for improvement in behavior. There were no significant changes in open field activity in treated WT mice, indicating that the dose used for treatment was not sedating (Figures 7A and 7B). However, risperidone decreased the activity levels of *Cntnap2*$^{-/-}$ mice to normal WT levels (Figures 7A and 7B). Consistent with the lack of a sedative effect, treated KO mice improved their nest-building score as well,

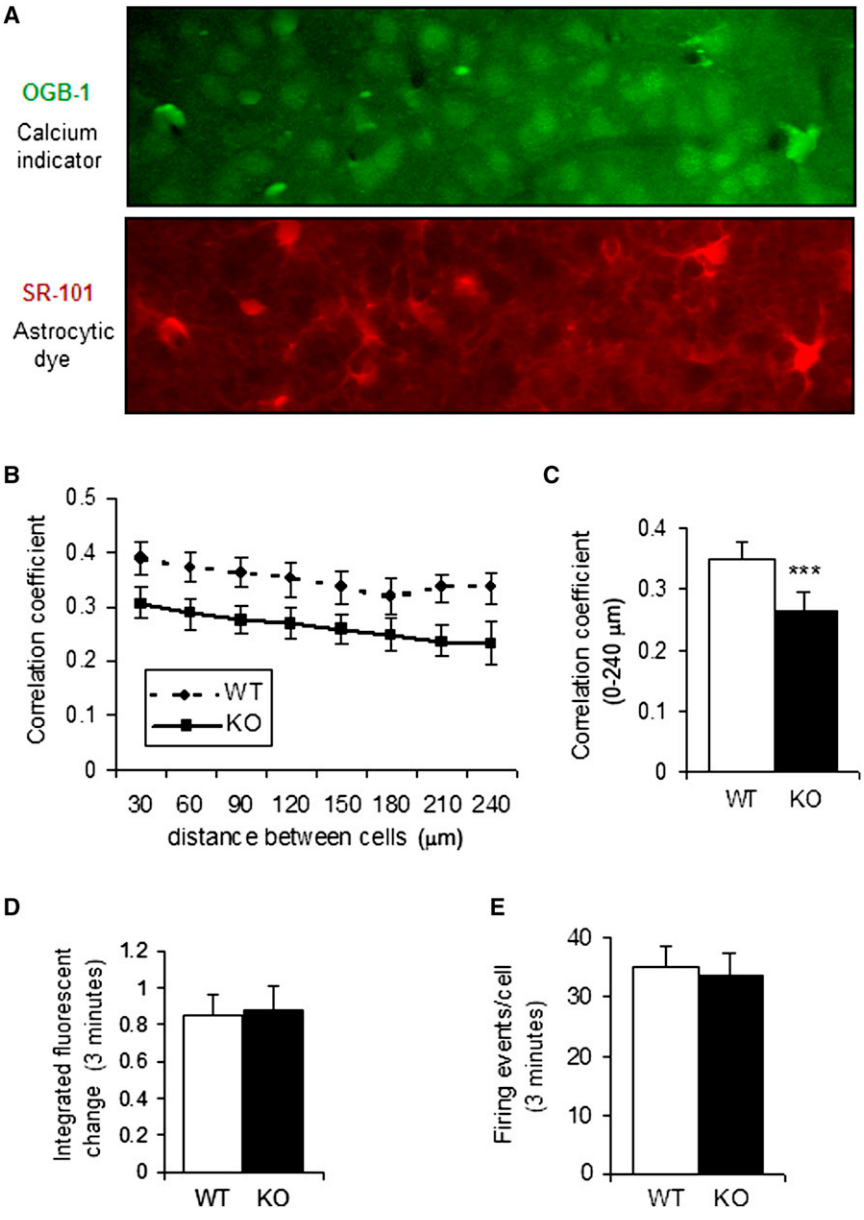

Figure 4. Reduced Neuronal Synchronization in *Cntnap2*$^{-/-}$ Mice

(A) Representative images of the calcium (top) and astrocytic (bottom) signals of a 3 min movie stack. OGB-1, Oregon green-1; SR-101, sulforhodamine-101.

(B) Correlation coefficient of neuronal firing for every pair of neurons over cell distance.

(C) Mean correlation coefficient over the distance range analyzed (240 μm).

(D) Firing amplitude presented as the summed fluorescence change across all imaged cells in a 3 min time window.

(E) Mean number of firing events per cell in a 3 min time window. n = 4 mice/genotype. Data are presented as mean ± SEM.

***p < 0.001.

a task that depends upon sustained activity (Figure 7C). Risperidone also reversed the increased grooming behavior of *Cntnap2*$^{-/-}$ mice (Figure 7E) and perseveration in the T maze (Figure 7F). To assess any effect of risperidone on social behavior, we performed the three- chamber social interaction test and found no improvement with treatment (Figure 7G); nor did we find improvement in sensory hypersensitivity (Figure 7D).

DISCUSSION

The development of mouse models of ASD is crucial to study the disorder at the molecular level, gain insight into disease mechanisms, and test potential pharmacological interventions. Here, we show that the consequences of CNTNAP2 deficiency in the mouse resemble many of the behavioral and cognitive features observed in patients with idiopathic autism and of the pathological features observed in patients with recessive *CNTNAP2* mutations that cause a Mendelian form of syndromic autism (Strauss et al., 2006). *Cntnap2*$^{-/-}$ mice have normal anxiety-related responses, visual spatial memory, and sensorimotor integration but show abnormal vocal communication, repetitive and restrictive behaviors, and abnormal social interactions. In addition, they also show hyperactivity and epileptic seizures, both features described in CDFE patients and in many patients with ASD. Heterozygous animals did not show any of the behavioral (Figure S5) or neuropathological (data not shown) abnormalities observed in homozygote knockouts; nor did they develop epileptic seizures, consistent with the recessive nature of the pathology in humans.

Autism and epilepsy are neurodevelopmental syndromes with a high frequency of co-occurrence (Geschwind, 2009), which suggests shared underlying mechanisms. At a molecular level, CNTNAP2 is a single pass transmembrane protein with a short cytoplasmic region involved in clustering K^+ channels at juxtaparanodes in myelinated axons (Horresh et al., 2008) and a long extracellular region that forms a neuron-glia cell adhesion complex with contactin 2 (CNTN2, also known as TAG-1), which is necessary for the proper localization of K^+ channels in this structure (Poliak et al., 2003). Thus, defects in myelination and K^+ channel mislocalization at the nodes of Ranvier could theoretically lead to epilepsy in *Cntnap2*$^{-/-}$ mice. However, this is not likely the case, as both light microscopic and ultrastructural analysis using electron microscopy in the peripheral and central nerves in CNTNAP2-deficient mice (Poliak et al., 2003) showed that nodal morphology and myelination were

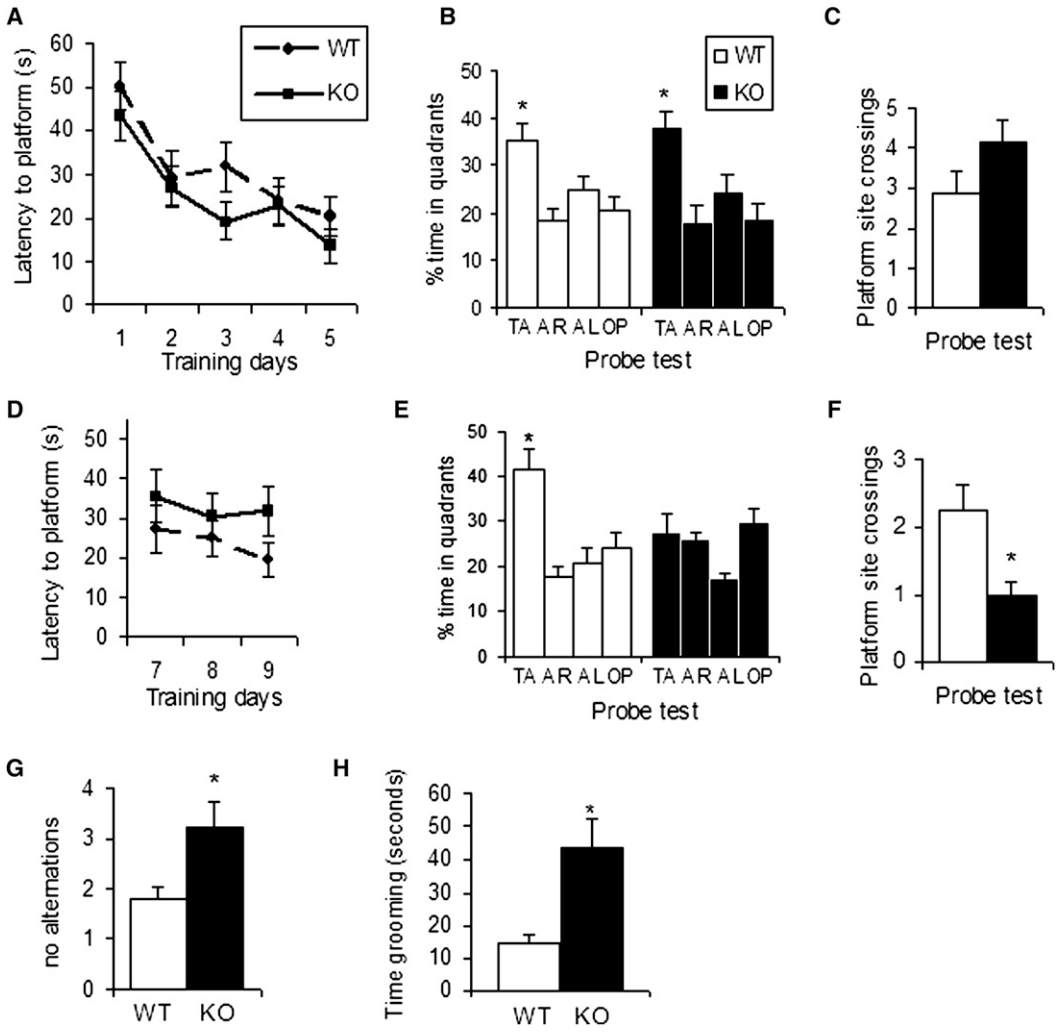

Figure 5. *Cntnap2*$^{-/-}$ Show Motor Stereotypic Movements and Behavioral Inflexibility

(A–F) Morris water maze (MWM) test. (A–C) Learning. (D–F) Reversal learning.

(A) Learning curve as indicated by the latency to locate a hidden platform (up to 60 s) during a 5 day training period. The average of four trials per day is presented.

(B) Probe test (the platform is removed), showing the percentage of time spent in each pool quadrant (in 60 s). Note that both genotypes spend significantly more time in the target quadrant. TA, target; AR, adjacent right; AL, adjacent left; OP, opposite.

(C) Number of platform site crossings during the probe test.

(D) Learning curve for the reversal task of the MWM test, showing the latency to locate the new platform.

(E) Probe test. Note that WT, but not KO, mice spend significantly more time in the target quadrant.

(F) Number of platform site crossings during the probe test.

(G) Number of no alternations in the T maze spontaneous alternation test (10 trials).

(H) Time spent grooming over a 10 min period.

*$p < 0.05$. n = 10 mice/genotype. Data are presented as mean ± SEM. See also Table S3 and Figure S4.

normal. In addition, electrophysiological investigation of nerve conductance revealed no abnormalities in conduction velocity, refractory period, or excitability (Poliak et al., 2003). In the current study, neuropathological analysis of *Cntnap2*$^{-/-}$ mice revealed two major mechanisms that have been shown to lead to epilepsy in humans, cortical neuronal migration abnormalities and a reduction in the number of GABAergic interneurons. Whereas neuronal migration abnormalities might have been expected based on observations in patients with CDFE syndrome, the reduction in GABAergic neurons was unexpected, as CNTNAP2 has not been previously associated with GABAergic neuronal function and no such deficit has been demonstrated in CDFE. These data suggest that assessment of interneurons in patients with CDFE would be worthwhile. Further, whether this reduction in interneurons is also due to a migration defect or, rather, to a defect in neurogenesis, differentiation, and/or survival remains to be elucidated in future work. Nevertheless, the embryonic expression of the gene in the ganglionic eminences and in

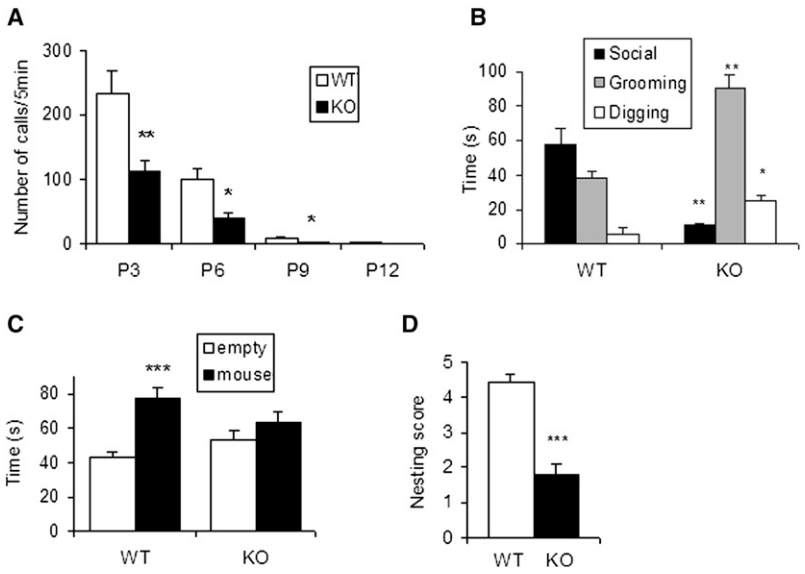

Figure 6. *Cntnap2*$^{-/-}$ Mice Show Communication and Social Behavior Abnormalities

(A) UsV. Number of calls from pups when separated from their mother at P3, P6, P9, and P12 (5 min).

(B) Juvenile play. Time involved in social interaction, as well as repetitive behaviors (grooming and digging) in pairs of mice matched in genotype and sex at age P21 (10 min).

(C) Three-chamber social interaction test. Time interacting with either an unfamiliar mouse or an inanimate object (empty cup) in 10 min.

(D) Nesting behavior. The nesting score represents the amount of nesting material used after a 16 hr period (1, poor; 5, good).

n = 10 mice/genotype. Data are presented as mean ± SEM. *$p < 0.05$, **$p < 0.01$, ***$p < 0.001$. See also Figure S5.

migrating interneurons supports a role for CNTNAP2 in the early development and migration of these cells.

The large extracellular domain of CNTNAP2 is composed of a number of protein-protein interaction domains that are common to cell adhesion molecules, including laminin G, EGF repeats, and discoidin-like domains (Poliak et al., 1999). During myelination, CNTNAP2 localizes to the developing nodes of Ranvier, where, as previously mentioned, it interacts extracellularly with CNTN2. Interestingly, CNTN2 is also expressed embryonically, and blocking its function results in migration abnormalities of cortical pioneer neurons and GABAergic interneurons (Denaxa et al., 2001; Morante-Oria et al., 2003), although normal numbers of interneurons were reported in CNTN2 deficient mice, likely due to compensatory mechanisms (Denaxa et al., 2005). Thus, analysis of CNTNAP2 interactors, including CNTN2, during embryogenesis could provide insight to the role of CNTNAP2 in neuronal migration.

One physiological consequence of the observed neuropathology caused by *Cntnap2* knockout is significantly reduced neuronal synchronization. It is generally accepted that most cognitive functions are based on the coordinated interactions of large neuronal ensembles within and across different specialized brain areas (Uhlhaas and Singer, 2006). Synchronization determines the pattern of neuronal interactions in a way that effective neuronal connectivity would diminish when synchronization is less precise (Womelsdorf et al., 2007). A number of functional neuroimaging studies have reported reduced connectivity in ASD (Just et al., 2004; Villalobos et al., 2005; Cherkassky et al., 2006; Damarla et al., 2010), supporting the notion that the deficits in cognition and behavior associated with ASD are most likely the result of a developmental disconnection (Geschwind and Levitt, 2007). Interestingly, we have recently associated common genetic risk variants in *CNTNAP2* with abnormal functional brain connectivity in humans (Scott-Van Zeeland et al., 2010). Our observations of migration abnormalities and reduced number of GABAergic interneurons in *Cntnap2*$^{-/-}$ mice, together with the normal global neuronal activity as measured by the firing rate and amplitude, suggest an abnormal neuronal circuit architecture as the cause of the asynchronous firing pattern, rather than abnormalities in neuronal function per se. There are a number of factors that contribute to the precise timing of neural activity (reviewed in Wang, 2010). Interestingly, GABAergic interneurons, in particular PVALB interneurons, have been reported to play a crucial role in the rhythmic pacing of cortical neuronal activity (Sohal et al., 2009). Therefore, further studies analyzing the structure of neuronal networks and interneuron function in *Cntnap2*$^{-/-}$ mice may have important implications for both the potential understanding and treatment of ASD.

The ultimate goal of understanding the pathophysiology of the disorder is to develop therapeutic interventions that improve or restore normal brain activity and, ultimately, the associated cognitive and behavioral deficits. Recent studies in mouse models are very encouraging in this regard, including Rett syndrome (Guy et al., 2007), fragile X syndrome (Dölen et al., 2007), neurofibromatosis type 1 (Costa et al., 2002), Down's syndrome (Fernandez et al., 2007), and tuberous sclerosis (Ehninger et al., 2008). Here, we have shown that risperidone efficiently reduces hyperactivity, motor stereotypies, and perseveration in *Cntnap2*$^{-/-}$ mice while having no effect on sociability. This observation provides evidence that different pathways lead to the ASD-associated core domains of social and repetitive behavior observed in this mouse model, parallel to the situation in humans, and supports the validity of this mouse model for testing new pharmacological treatments.

Repetitive behavior is recognized as reflecting a disruption of the coordinated function of the cortico-striatal circuit (Albin et al., 1989). In brief, two main pathways compose this system: the direct pathway, which promotes motor behavior, and the indirect pathway, which inhibits it (Gerfen et al., 1990). In general, stereotypies indicate an unbalanced activity of this network favoring the direct pathway (Lewis et al., 2007). At the neuronal level, the ultimate firing output to the direct and indirect pathways is determined by excitatory inputs from cortex and thalamus and inhibitory inputs from local interneurons within the striatum (Kreitzer and Malenka, 2008). Interestingly, PVALB+ fast-spiking interneurons, which are the main source of inhibitory input in

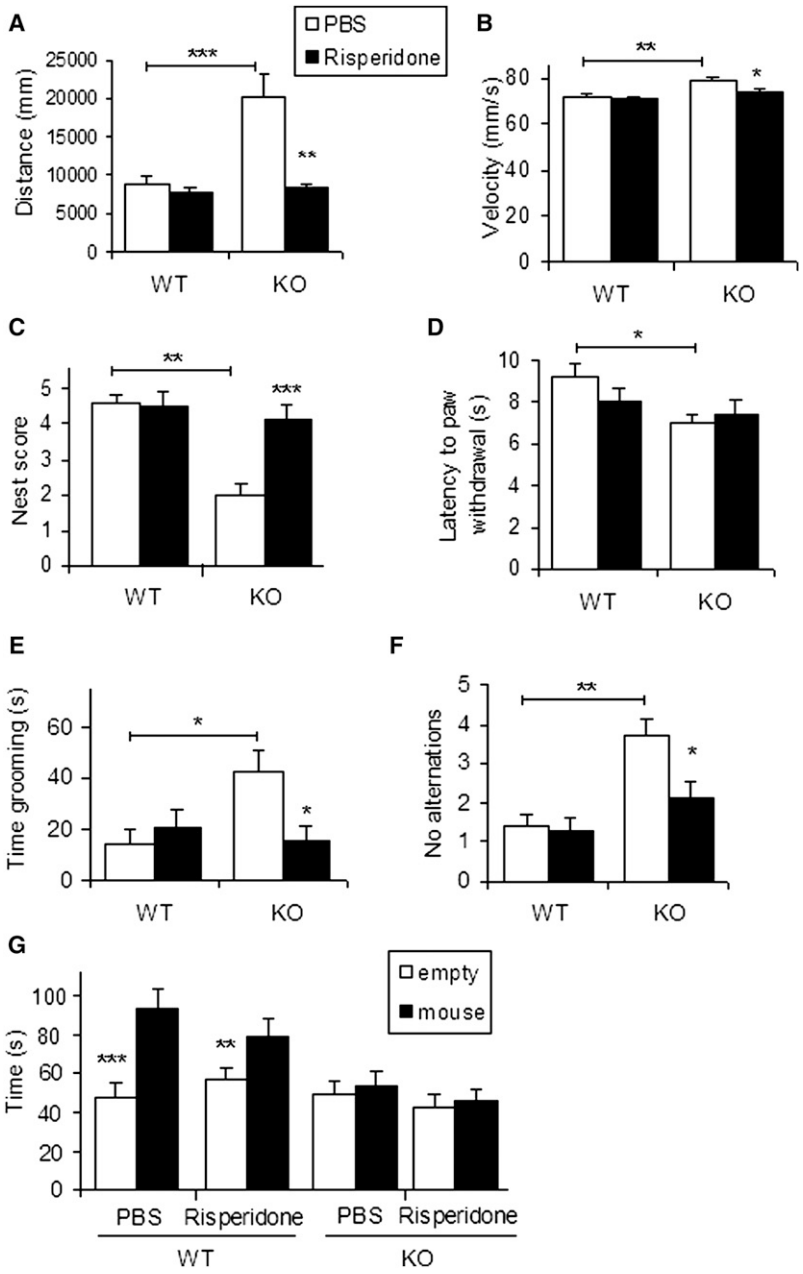

Figure 7. Risperidone Rescues Hyperactivity and Repetitive Behavior/Perseveration in *Cntnap2*$^{-/-}$ Mice

(A and B) Open field test. Distance traveled (A) and velocity (B) for vehicle- (PBS) and drug-treated WT and KO mice (20 min).

(C) Nesting behavior. Risperidone improves the nesting score of *Cntnap2*$^{-/-}$ mice.

(D) Hot plate. Risperidone did not have an effect in the hyperreactivity to thermal stimuli.

(E) Grooming behavior is reduced in risperidone-treated mutant mice (10 min).

(F) Risperidone improved spontaneous alternation of mutant mice.

(G) Drug treatment did not have an effect in the three-chamber social interaction test.

n = 10 mice/genotype and treatment condition. Data are presented as mean ± SEM. *p < 0.05, **p < 0.01, ***p < 0.001.

the cortico-striatal circuit, have recently been shown to target mainly the direct pathway (Gittis et al., 2010). Therefore, the reduced number of this type of interneuron in *Cntnap2*$^{-/-}$ mice likely results in overactivation of this pathway, leading to hyperactivity and repetitive behavior. Indeed, risperidone is known to potentiate the indirect pathway, which likely rebalances the activity of this network, alleviating these behaviors.

Nest building has also been shown to be related to the dopaminergic pathway (Szczypka et al., 2001) and has been reported as disrupted in mice with hyperactivity (Kwon et al., 2006; Zhou et al., 2010). That risperidone also normalized the nesting ability in KO mice provides additional evidence for abnormal striatal dopaminergic function in this model. Exploration of cortico-striatal function in *Cntnap2*$^{-/-}$ mice will provide a better understanding of the neural basis of repetitive behavior in ASD. In addition, the dissociation between repetitive and social behavior with regards to treatment response suggests that *Cntnap2*$^{-/-}$ mice will be useful for dissecting the distinct circuitries involved in these core components of autistic-related abnormal behavior. Finally, because understanding of CNTNAP2 function was previously focused primarily on postnatal development, these data set a new direction for investigation of CNTNAP2's role during development and in the formation and function of neuronal circuits.

EXPERIMENTAL PROCEDURES

Mice

Cntnap2 mutant and WT mice were obtained from heterozygous crossings and were born with the expected Mendelian frequencies. The day of vaginal plug detection was designated as E0.5 and the day of birth as P0. The three obtained genotypes were housed together with three to four same sex mice per cage. They were kept in 12 hr light/12 hr dark cycle and had *ad-lib* access to food and water. All procedures involving animals were performed in accordance with the UCLA animal research committee.

Western Blot, In Situ Hybridization, and Immunohistochemistry

Western blot, in situ hybridization, and immunohistochemistry were performed using standard methods. See Extended Experimental Procedures for details.

BrdU Labeling

Timed pregnant mice (E16.5) received a single i.p. injection of BrdU (50 mg/kg body weight, Sigma).

Imaging and Cell Counts

Images were acquired with a Zeiss LSM-510 laser-scanning confocal microscope. Eight anatomically matched sections from at least three mice per

genotype were selected for cell counting. For cortical images, cells were counted in matched areas of fixed size (1.2 mm wide) in each hemisphere of somatosensory cortex. The boundaries of the different cortical layers were determined by counterstaining each section with DAPI.

Weighted Gene Coexpression Network Analysis

The original microarray data set was deposited by Sugino et al. (2006) in the Gene Expression Omnibus (http://www.ncbi.nlm.nih.gov/geo/query/acc.cgi?acc=GSE2882). Weighted gene coexpression network analysis (WGCNA) was performed as previously described (Winden et al., 2009). More detailed conditions are included in the Extended Experimental Procedures.

Electroencephalographic Recordings

Mice were deeply anesthetized with isoflurane, and microelectrodes (0.005 inch diameter) were implanted over right frontal and parietal cortices. Mice were allowed to recover for 48 hr, and EEG activity was recorded daily for up to 2 weeks.

In Vivo Two-Photon Calcium Imaging

Neuronal activity was imaged using a calcium indicator injected in layer II/III of somatosensory cortex in young adult mice (2–4 months of age). See the Extended Experimental Procedures for details.

Behavioral Tests

Ten mice per genotype were evaluated for each behavioral test. Mice were tagged with either an ear tag number or a toe tattoo (in the case of pups). Experimenters were blinded to the genotype during testing. Behavioral tests were performed in the UCLA behavioral test core and analyzed with TopScan (Clever Sys, Inc.) automated system. UsV were analyzed with Avisoft sound analysis and synthesis software for laboratory animals.

Morris Water Maze

The MWM test was performed as described elsewhere (Vorhees and Williams, 2006). In brief, mice were trained to locate a hidden platform based on distal visual cues to escape from the pool. Mice received four training trials per day (with different start points) for 5 consecutive days. On day 6, the platform was removed and a probe test was performed. The next day, the platform was moved to the opposite quadrant and the reversal task of the test was started. Mice received again four training trials per day to locate the new platform. A probe test was performed on day 10.

T Maze Spontaneous Alternation

Mice were placed on the base of a T maze and were given the choice to explore either the right or left arm of the maze for ten consecutive trials. A choice was assumed to be made when the mice stepped with the four paws into an arm. At that moment, the gate to that arm was closed and the animal was allowed to explore the arm for 5 s.

Ultrasonic Vocalization

Pups were removed from the dam and placed in individual heated sound proof chambers equipped to record ultrasonic vocalization (UsV) for 5 min. To avoid potential confounding effects due to temperature, the room was maintained at 21°C and body temperature was measured with a rectal probe after 5 min of the test at P6 (~35°C in both genotypes).

Juvenile Play

Mice at age P21 were placed in a cage (previously habituated to it) with an unfamiliar mouse matched in genotype and sex for 10 min. The time mice were engaged in social interaction (nose-to-nose sniffing, nose-to-anus sniffing, following or crawling on/under each other), and the time mice spent engaged in repetitive behaviors (grooming and digging) was measured by a human observer (Silverman et al., 2010).

Three-Chamber Social Interaction Test

The social interaction test was performed as previously described (Silverman et al., 2010). In brief, after habituation, a mouse was placed in the central chamber of a clear Plexiglas box divided into three interconnected chambers and was given the choice to interact with either an empty wire cup (located in one side chamber) or a similar wire cup with an unfamiliar mouse inside (located in the opposite chamber). Time sniffing each cup was measured.

Drug Administration

Risperidone (0.2 mg/kg, Sigma) was administered by a daily i.p. injection in a volume of 10 ml/kg for 7 consecutive days. Behavioral tests were performed on days 8, 9, and 10. Mice also received drug treatment during these days approximately 1 hr prior to testing.

Statistical Analyses

All results are expressed as mean ± SEM. For cell quantifications and neuronal synchrony comparisons between groups, a one-way ANOVA was used. To compare cell distributions within the cortical layers, we used two-way ANOVA. For behavioral tests, either one- or two-way ANOVA with repeated measures followed by Bonferroni-Dunn posthoc tests, when applied, were used.

SUPPLEMENTAL INFORMATION

Supplemental Information includes Extended Experimental Procedures, five figures, three tables, and one movie and can be found with this article online at doi:10.1016/j.cell.2011.08.040.

ACKNOWLEDGMENTS

We thank the UCLA behavioral testing core and its supervisor, Dr. Ravi Ponnusamy, for assistance with behavioral testing. We also thank Dr. Alcino Silva, codirector of the core, for his critical discussions about mouse behavioral testing; Dr. Stephanie White for the UsV equipment and software; Dr. Carolyn Houser for assistance with GAD1 IHC; and Dr. William Yang and Dr. Istvan Mody for helpful discussions. We would also like to thank Jamee Bomar and Dr. Asami Oguro-Ando for help with floating IHC and helpful discussions; Greg Osborn for help with UsV analysis; Clark Rosensweig for help with mouse genotyping; Dr. Irina Voineagu and Lauren Kawaguchi for critically reading the manuscript; and Dr. Eric Wexler for useful discussions on drug treatment. This work was supported by grants NIH/NIMH R01 MH081754-02R to D.H.G.; NIH ACE Center 1P50-HD055784-01 to D.H.G. (Project II) and Network grant 5R01-MH081754-04 to D.H.G.; NIH/NS50220 to E.P.; and Dr. Miriam and Sheldon G. Adelson Medical Research Foundation to D.H.G. and E.P. E.P. is the Incumbent of the Hanna Hertz Professorial Chair for Multiple Sclerosis and Neuroscience.

Received: April 6, 2011
Revised: June 28, 2011
Accepted: August 26, 2011
Published: September 29, 2011

REFERENCES

Abrahams, B.S., Tentler, D., Perederiy, J.V., Oldham, M.C., Coppola, G., and Geschwind, D.H. (2007). Genome-wide analyses of human perisylvian cerebral cortical patterning. Proc. Natl. Acad. Sci. USA *104*, 17849–17854.

Alarcón, M., Abrahams, B.S., Stone, J.L., Duvall, J.A., Perederiy, J.V., Bomar, J.M., Sebat, J., Wigler, M., Martin, C.L., Ledbetter, D.H., et al. (2008). Linkage, association, and gene-expression analyses identify *CNTNAP2* as an autism-susceptibility gene. Am. J. Hum. Genet. *82*, 150–159.

Albin, R.L., Young, A.B., and Penney, J.B. (1989). The functional anatomy of basal ganglia disorders. Trends Neurosci. *12*, 366–375.

Angevine, J.B., Jr., and Sidman, R.L. (1961). Autoradiographic study of cell migration during histogenesis of cerebral cortex in the mouse. Nature *192*, 766–768.

APA (American Psychiatric Association). (2000). Diagnostic and Statistical Manual of Mental Disorders, Fourth Edition (Washington, DC: American Psychiatric Publishing).

Arking, D.E., Cutler, D.J., Brune, C.W., Teslovich, T.M., West, K., Ikeda, M., Rea, A., Guy, M., Lin, S., Cook, E.H., and Chakravarti, A. (2008). A common genetic variant in the neurexin superfamily member CNTNAP2 increases familial risk of autism. Am. J. Hum. Genet. *82*, 160–164.

Bakkaloglu, B., O'Roak, B.J., Louvi, A., Gupta, A.R., Abelson, J.F., Morgan, T.M., Chawarska, K., Klin, A., Ercan-Sencicek, A.G., Stillman, A.A., et al. (2008). Molecular cytogenetic analysis and resequencing of contactin associated protein-like 2 in autism spectrum disorders. Am. J. Hum. Genet. *82*, 165–173.

Belmonte, M.K., Allen, G., Beckel-Mitchener, A., Boulanger, L.M., Carper, R.A., and Webb, S.J. (2004). Autism and abnormal development of brain connectivity. J. Neurosci. *24*, 9228–9231.

Chadman, K.K., Yang, M., and Crawley, J.N. (2009). Criteria for validating mouse models of psychiatric diseases. Am. J. Med. Genet. B. Neuropsychiatr. Genet. *150B*, 1–11.

Cherkassky, V.L., Kana, R.K., Keller, T.A., and Just, M.A. (2006). Functional connectivity in a baseline resting-state network in autism. Neuroreport *17*, 1687–1690.

Costa, R.M., Federov, N.B., Kogan, J.H., Murphy, G.G., Stern, J., Ohno, M., Kucherlapati, R., Jacks, T., and Silva, A.J. (2002). Mechanism for the learning deficits in a mouse model of neurofibromatosis type 1. Nature *415*, 526–530.

Crawley, J.N. (2007). Mouse behavioral assays relevant to the symptoms of autism. Brain Pathol. *17*, 448–459.

Damarla, S.R., Keller, T.A., Kana, R.K., Cherkassky, V.L., Williams, D.L., Minshew, N.J., and Just, M.A. (2010). Cortical underconnectivity coupled with preserved visuospatial cognition in autism: Evidence from an fMRI study of an embedded figures task. Autism Res. *3*, 273–279.

Deacon, R.M. (2006). Assessing nest building in mice. Nat. Protoc. *1*, 1117–1119.

Denaxa, M., Chan, C.H., Schachner, M., Parnavelas, J.G., and Karagogeos, D. (2001). The adhesion molecule TAG-1 mediates the migration of cortical interneurons from the ganglionic eminence along the corticofugal fiber system. Development *128*, 4635–4644.

Denaxa, M., Kyriakopoulou, K., Theodorakis, K., Trichas, G., Vidaki, M., Takeda, Y., Watanabe, K., and Karagogeos, D. (2005). The adhesion molecule TAG-1 is required for proper migration of the superficial migratory stream in the medulla but not of cortical interneurons. Dev. Biol. *288*, 87–99.

Dölen, G., Osterweil, E., Rao, B.S., Smith, G.B., Auerbach, B.D., Chattarji, S., and Bear, M.F. (2007). Correction of fragile X syndrome in mice. Neuron *56*, 955–962.

Ehninger, D., Han, S., Shilyansky, C., Zhou, Y., Li, W., Kwiatkowski, D.J., Ramesh, V., and Silva, A.J. (2008). Reversal of learning deficits in a Tsc2+/- mouse model of tuberous sclerosis. Nat. Med. *14*, 843–848.

Fernandez, F., Morishita, W., Zuniga, E., Nguyen, J., Blank, M., Malenka, R.C., and Garner, C.C. (2007). Pharmacotherapy for cognitive impairment in a mouse model of Down syndrome. Nat. Neurosci. *10*, 411–413.

Gerfen, C.R., Engber, T.M., Mahan, L.C., Susel, Z., Chase, T.N., Monsma, F.J., Jr., and Sibley, D.R. (1990). D1 and D2 dopamine receptor-regulated gene expression of striatonigral and striatopallidal neurons. Science *250*, 1429–1432.

Gerlai, R., Pisacane, P., and Erickson, S. (2000). Heregulin, but not ErbB2 or ErbB3, heterozygous mutant mice exhibit hyperactivity in multiple behavioral tasks. Behav. Brain Res. *109*, 219–227.

Geschwind, D.H. (2009). Advances in autism. Annu. Rev. Med. *60*, 367–380.

Geschwind, D.H., and Levitt, P. (2007). Autism spectrum disorders: developmental disconnection syndromes. Curr. Opin. Neurobiol. *17*, 103–111.

Gittis, A.H., Nelson, A.B., Thwin, M.T., Palop, J.J., and Kreitzer, A.C. (2010). Distinct roles of GABAergic interneurons in the regulation of striatal output pathways. J. Neurosci. *30*, 2223–2234.

Glessner, J.T., Wang, K., Cai, G., Korvatska, O., Kim, C.E., Wood, S., Zhang, H., Estes, A., Brune, C.W., Bradfield, J.P., et al. (2009). Autism genome-wide copy number variation reveals ubiquitin and neuronal genes. Nature *459*, 569–573.

Guy, J., Gan, J., Selfridge, J., Cobb, S., and Bird, A. (2007). Reversal of neurological defects in a mouse model of Rett syndrome. Science *315*, 1143–1147.

Horresh, I., Poliak, S., Grant, S., Bredt, D., Rasband, M.N., and Peles, E. (2008). Multiple molecular interactions determine the clustering of Caspr2 and Kv1 channels in myelinated axons. J. Neurosci. *28*, 14213–14222.

Inda, M.C., DeFelipe, J., and Muñoz, A. (2006). Voltage-gated ion channels in the axon initial segment of human cortical pyramidal cells and their relationship with chandelier cells. Proc. Natl. Acad. Sci. USA *103*, 2920–2925.

Just, M.A., Cherkassky, V.L., Keller, T.A., and Minshew, N.J. (2004). Cortical activation and synchronization during sentence comprehension in high-functioning autism: evidence of underconnectivity. Brain *127*, 1811–1821.

Kreitzer, A.C., and Malenka, R.C. (2008). Striatal plasticity and basal ganglia circuit function. Neuron *60*, 543–554.

Kwon, C.H., Luikart, B.W., Powell, C.M., Zhou, J., Matheny, S.A., Zhang, W., Li, Y., Baker, S.J., and Parada, L.F. (2006). Pten regulates neuronal arborization and social interaction in mice. Neuron *50*, 377–388.

Levitt, P., Eagleson, K.L., and Powell, E.M. (2004). Regulation of neocortical interneuron development and the implications for neurodevelopmental disorders. Trends Neurosci. *27*, 400–406.

Lewis, M.H., Tanimura, Y., Lee, L.W., and Bodfish, J.W. (2007). Animal models of restricted repetitive behavior in autism. Behav. Brain Res. *176*, 66–74.

Marín, O., Yaron, A., Bagri, A., Tessier-Lavigne, M., and Rubenstein, J.L. (2001). Sorting of striatal and cortical interneurons regulated by semaphorin-neuropilin interactions. Science *293*, 872–875.

McDougle, C.J., Scahill, L., McCracken, J.T., Aman, M.G., Tierney, E., Arnold, L.E., Freeman, B.J., Martin, A., McGough, J.J., Cronin, P., et al. (2000). Research Units on Pediatric Psychopharmacology (RUPP) Autism Network. Background and rationale for an initial controlled study of risperidone. Child Adolesc. Psychiatr. Clin. N. Am. *9*, 201–224.

McDougle, C.J., Stigler, K.A., Erickson, C.A., and Posey, D.J. (2008). Atypical antipsychotics in children and adolescents with autistic and other pervasive developmental disorders. J. Clin. Psychiatry *69* (*Suppl 4*), 15–20.

Molyneaux, B.J., Arlotta, P., Menezes, J.R., and Macklis, J.D. (2007). Neuronal subtype specification in the cerebral cortex. Nat. Rev. Neurosci. *8*, 427–437.

Morante-Oria, J., Carleton, A., Ortino, B., Kremer, E.J., Fairén, A., and Lledo, P.M. (2003). Subpallial origin of a population of projecting pioneer neurons during corticogenesis. Proc. Natl. Acad. Sci. USA *100*, 12468–12473.

Nakatani, J., Tamada, K., Hatanaka, F., Ise, S., Ohta, H., Inoue, K., Tomonaga, S., Watanabe, Y., Chung, Y.J., Banerjee, R., et al. (2009). Abnormal behavior in a chromosome-engineered mouse model for human 15q11-13 duplication seen in autism. Cell *137*, 1235–1246.

Nestler, E.J., and Hyman, S.E. (2010). Animal models of neuropsychiatric disorders. Nat. Neurosci. *13*, 1161–1169.

Oldham, M.C., Konopka, G., Iwamoto, K., Langfelder, P., Kato, T., Horvath, S., and Geschwind, D.H. (2008). Functional organization of the transcriptome in human brain. Nat. Neurosci. *11*, 1271–1282.

Poliak, S., Gollan, L., Martinez, R., Custer, A., Einheber, S., Salzer, J.L., Trimmer, J.S., Shrager, P., and Peles, E. (1999). Caspr2, a new member of the neurexin superfamily, is localized at the juxtaparanodes of myelinated axons and associates with K+ channels. Neuron *24*, 1037–1047.

Poliak, S., Salomon, D., Elhanany, H., Sabanay, H., Kiernan, B., Pevny, L., Stewart, C.L., Xu, X., Chiu, S.Y., Shrager, P., et al. (2003). Juxtaparanodal clustering of Shaker-like K+ channels in myelinated axons depends on Caspr2 and TAG-1. J. Cell Biol. *162*, 1149–1160.

Racine, R.J. (1972). Modification of seizure activity by electrical stimulation. II. Motor seizure. Electroencephalogr. Clin. Neurophysiol. *32*, 281–294.

Scott-Van Zeeland, A.A., Abrahams, B.S., Alvarez-Retuerto, A.I., Sonnenblick, L.I., Rudie, J.D., Ghahremani, D., Mumford, J.A., Poldrack, R.A., Dapretto, M., Geschwind, D.H., and Bookheimer, S.Y. (2010). Altered functional connectivity in frontal lobe circuits is associated with variation in the autism risk gene CNTNAP2. Sci. Transl. Med. *2*, ra80.

Scattoni, M.L., Crawley, J., and Ricceri, L. (2009). Ultrasonic vocalizations: a tool for behavioural phenotyping of mouse models of neurodevelopmental disorders. Neurosci. Biobehav. Rev. *33*, 508–515.

Sebat, J., Lakshmi, B., Malhotra, D., Troge, J., Lese-Martin, C., Walsh, T., Yamrom, B., Yoon, S., Krasnitz, A., Kendall, J., et al. (2007). Strong association of de novo copy number mutations with autism. Science *316*, 445–449.

Silverman, J.L., Yang, M., Lord, C., and Crawley, J.N. (2010). Behavioural phenotyping assays for mouse models of autism. Nat. Rev. Neurosci. *11*, 490–502.

Sohal, V.S., Zhang, F., Yizhar, O., and Deisseroth, K. (2009). Parvalbumin neurons and gamma rhythms enhance cortical circuit performance. Nature *459*, 698–702.

Strauss, K.A., Puffenberger, E.G., Huentelman, M.J., Gottlieb, S., Dobrin, S.E., Parod, J.M., Stephan, D.A., and Morton, D.H. (2006). Recessive symptomatic focal epilepsy and mutant contactin-associated protein-like 2. N. Engl. J. Med. *354*, 1370–1377.

Sugino, K., Hempel, C.M., Miller, M.N., Hattox, A.M., Shapiro, P., Wu, C., Huang, Z.J., and Nelson, S.B. (2006). Molecular taxonomy of major neuronal classes in the adult mouse forebrain. Nat. Neurosci. *9*, 99–107.

Szczypka, M.S., Kwok, K., Brot, M.D., Marck, B.T., Matsumoto, A.M., Donahue, B.A., and Palmiter, R.D. (2001). Dopamine production in the caudate putamen restores feeding in dopamine-deficient mice. Neuron *30*, 819–828.

Uhlhaas, P.J., and Singer, W. (2006). Neural synchrony in brain disorders: relevance for cognitive dysfunctions and pathophysiology. Neuron *52*, 155–168.

Vernes, S.C., Newbury, D.F., Abrahams, B.S., Winchester, L., Nicod, J., Groszer, M., Alarcón, M., Oliver, P.L., Davies, K.E., Geschwind, D.H., et al. (2008). A functional genetic link between distinct developmental language disorders. N. Engl. J. Med. *359*, 2337–2345.

Villalobos, M.E., Mizuno, A., Dahl, B.C., Kemmotsu, N., and Müller, R.A. (2005). Reduced functional connectivity between V1 and inferior frontal cortex associated with visuomotor performance in autism. Neuroimage *25*, 916–925.

Vitali, R., and Clarke, S. (2004). Improved rotorod performance and hyperactivity in mice deficient in a protein repair methyltransferase. Behav. Brain Res. *153*, 129–141.

Vorhees, C.V., and Williams, M.T. (2006). Morris water maze: procedures for assessing spatial and related forms of learning and memory. Nat. Protoc. *1*, 848–858.

Wang, X.J. (2010). Neurophysiological and computational principles of cortical rhythms in cognition. Physiol. Rev. *90*, 1195–1268.

Weiss, L.A., Arking, D.E., Gene Discovery Project of Johns Hopkins & the Autism Consortium, Daly, M.J., and Chakravarti, A. (2009). A genome-wide linkage and association scan reveals novel loci for autism. Nature *461*, 802–808.

Winden, K.D., Oldham, M.C., Mirnics, K., Ebert, P.J., Swan, C.H., Levitt, P., Rubenstein, J.L., Horvath, S., and Geschwind, D.H. (2009). The organization of the transcriptional network in specific neuronal classes. Mol. Syst. Biol. *5*, 291–308.

Wonders, C.P., and Anderson, S.A. (2006). The origin and specification of cortical interneurons. Nat. Rev. Neurosci. *7*, 687–696.

Womelsdorf, T., Schoffelen, J.M., Oostenveld, R., Singer, W., Desimone, R., Engel, A.K., and Fries, P. (2007). Modulation of neuronal interactions through neuronal synchronization. Science *316*, 1609–1612.

Zhang, B., and Horvath, S. (2005). A general framework for weighted gene coexpression network analysis. Stat. Appl. Genet. Mol. Biol. *4*, 17.

Zhou, M., Rebholz, H., Brocia, C., Warner-Schmidt, J.L., Fienberg, A.A., Nairn, A.C., Greengard, P., and Flajolet, M. (2010). Forebrain overexpression of CK1δ leads to down-regulation of dopamine receptors and altered locomotor activity reminiscent of ADHD. Proc. Natl. Acad. Sci. USA *107*, 4401–4406.

Cell

EXTENDED EXPERIMENTAL PROCEDURES

Western Blot

Whole brains from WT and KO mice were dissected and homogenized to obtain the specific brain lysates. Proteins were fractionated by SDS/PAGE and immunoblotted with rabbit anti CNTNAP2 (1:200, Millipore) and mouse anti GAPDH (1:250, Abcam) to standardize protein loading between samples. Appropriate IgG antibodies conjugated with horseradish peroxidase were used as secondary antibody.

In Situ Hybridization

In situ hybridization was performed on fresh frozen tissues as previously described (Abrahams et al., 2007). The *Cntnap2* probe corresponds to nucleotides 191-667 of the mouse *Cntnap2* cDNA (GenBank 52138537).

Immunohistochemistry

Mice were deeply anesthetized with Nembutal (sodium pentobarbital, 40 mg/kg body weight) and perfused intracardially with 4% paraformaldehyde (PFA) in phosphate-buffered solution (PBS). The brains were removed, postfixed overnight in the same fixative and cryoprotected by immersion in 30% sucrose for 3-5 days. Brains were embedded in OCT, sectioned at a thickness of 40 μm on a cryostat and used for free-floating IHC using standard methods. Incubations with primary antibodies were performed overnight at 4°C and with secondary antibodies for 90 min at room temperature. For primary antibodies we used mouse anti NeuN (1:500, Millipore), rabbit anti GFAP (1:500, Abcam), rabbit anti CUX1 (1:200, Santa Cruz), rabbit anti FOXP2 (1:200, Sigma), rat anti BrdU (1:100, Abcam), mouse anti GAD1 (1:1500, Millipore), rabbit anti PVALB (1:250, Immunostar), rabbit anti CALB2 (1:100, Abcam), rabbit anti NPY (1:4000, Abcam), sheep anti CHAT (1:500, Abcam). Appropriate secondary antibodies were from the Alexafluor series from Invitrogen. IHC on BrdU labeled sections was performed as previously described after incubating sections in 2N HCl for 30 min at 37°C to denature DNA.

Weighted Gene Coexpression Network Analysis

Raw microarray data from Sugino et al. (2006) were analyzed as in Winden et al. (2009). Briefly, genes with consistent presence in at least one cell type, high coefficient of variation (40.21), and high connectivity (k40.11) were selected for network construction. These genes were clustered based on their topological overlap (TO), which considers the correlation of two genes with each other as well as the degree of their shared correlation within the network (Zhang and Horvath, 2005). Modules (with a minimum of 50 genes) were identified using an automatic module detection algorithm (Langfelder et al., 2008). To visualize the pairwise relationships between genes, we used the software VisANT (http://visant.bu.edu/). The 300 strongest connections were depicted.

In Vivo Two-Photon Calcium Imaging

Young adult mice (2-4 months of age, 4 mice/genotype) were sedated with 10 mg/kg Chlorprothixene (Sigma) in DMSO, the skull was removed and a calcium indicator solution (1 mM Oregon-Green BAPTA-1 AM, Invitrogen) and Sulforhodamine-101 (100 μM, Invitrogen), to visualize astrocytes, were injected at a depth of 250 μm below the dura through 4 Mohmn glass pipettes over 1 min with a pressure of 10 PSI using a Picospritzer. The skull was replaced with a 3 mm diameter glass coverslip. Mice were transferred to the microscope stage, head-fixed and kept under light isoflurane anesthesia (0.25%) at 37°C using a temperature control device. Calcium imaging was begun ~1 hr after injection. Images of layer II/III neurons in somatosensory cortex were obtained using 4Hz line scan with a custom-built 2-photon laser-scanning microscope with a Ti:Sapphire pulsed laser (SpectraPhysics Mai Tai BB) tuned to 870 nm. Three minutes movies were acquired using ScanImage software (Pologruto et al., 2003). Astrocytic signals were excluded from the analysis. Neuronal somatic calcium transients were detected using a well-established temporal deconvolution algorithm (Yaksi and Friedrich, 2006). To quantify neuronal synchronization, we computed pair-wise correlation coefficients for all possible pairs of neurons from the deconvolved calcium traces as in Golshani et al. (2009). The number of these transients, as estimation of firing rate, as well as their amplitude were calculated from changes in the fluorescence signal.

Open Field

Mice were placed inside a clear plexiglass arena (27.5cm x 27.5cm) for 20 min and their general activity was recorded.

Rotorod

Mice were subjected to two consecutive tests for up to 180 s each. The first was at constant speed (60 rpm), which was reached in 10 s and maintained until the end of the test, and the second at accelerating speed (0-120 rpm), where the maximum speed was reached in 60 s and maintained until the end of the test. The latency to fall (or rotate grasping the rotorod bar in some cases) in each test was measured as indicative of motor balance and coordination.

Light-Dark Box

Mice were placed in a box with a small dark safe compartment and a large aversive compartment illuminated with bright light for 10 min. The time spent in the bright area was measured as indicative of their anxiety levels.

Acoustic Startle and PPI

Mice were placed in a restraint tube mounted on a startle measurement platform. For the acoustic startle, the response to a stimulus of loud noise (120 dB) was recorded. To determine the degree of PPI, the startle-eliciting stimulus (120 dB sound) was preceded by a brief low-intensity stimulus of 70 dB, 75 dB or 80 dB and the new startle response at each intensity level was measured. The specific pattern of pulse and prepulse sounds used and the PPI calculation formula are described in Geyer and Dulawa (2003).

Olfaction

Olfaction was assessed by measuring latency to find a buried piece of food in a cage to which mice had been previously habituated, as described by Yang and Crawley (2009).

Grooming

Mice were individually caged and the time spent grooming during a 10 min period was measured.

Nest Building

The nest score (1 to 5) was calculated as proposed by Deacon (2006). Briefly, two main parameters were taken into account: first, the amount of cotton material used after 16h and second, the shape and height of the nest.

SUPPLEMENTAL REFERENCES

Geyer, M.A., and Dulawa S.C. (2003). Assessment of murine startle reactivity, prepulse inhibition, and habituation. Curr. Protoc. Neurosci. *8*, Unit 8.17.

Golshani, P., Gonçalves, J.T., Khoshkhoo, S., Mostany, R., Smirnakis, S., and Portera-Cailliau, C. (2009). Internally mediated developmental desynchronization of neocortical network activity. J. Neurosci. *29*, 10890–10899.

Langfelder, P., Zhang, B., and Horvath, S. (2008). Defining clusters from a hierarchical cluster tree: the Dynamic Tree Cut package for R. Bioinformatics *24*, 719–720.

Pologruto, T.A., Sabatini, B.L., and Svoboda, K. (2003). ScanImage: flexible software for operating laser scanning microscopes. Biomed. Eng. Online *2*, 13.

Yang, M., Crawley, J.N. (2009). Simple behavioral assessment of mouse olfaction. Curr. Protoc. Neurosci. *8*, Unit 8.24.

Yaksi, E., and Friedrich, R.W. (2006). Reconstruction of firing rate changes across neuronal populations by temporally deconvolved $Ca2^{+}$ imaging. Nat. Methods *3*, 377–383.

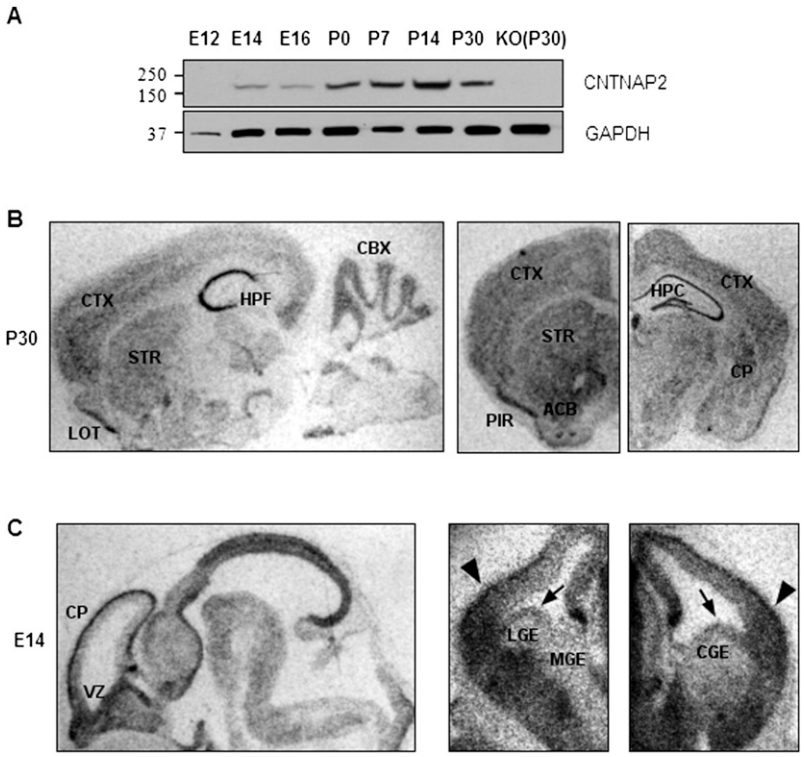

Figure S1. Expression of *Cntnap2* in Mouse Brain, Related to Figure 2 and Figure 3

(A) Western blot of CNTNAP2 expression during development.

(B) In situ hybridization of *Cntnap2* in adult WT mice. CTX, cortex; STR, striatum; LOT, lateral olfactory tract; HPF, hippocampal formation; CBX, cerebellar cortex; PIR, piriform cortex; ACB nucleus accumbens; CP, caudate putamen.

(C) In situ hybridization of *Cntnap2* in WT embryos. CP, cortical plate; VZ, ventricular zone; LGE, lateral ganglionic eminence; MGE, medial ganglionic eminence; CGE, caudal ganglionic eminence. Arrows show expression of *Cntnap2* in the ganglionic eminences, arrowheads show expression of the gene in regions that contain migrating interneurons. n = 3 embryos/mice for each age.

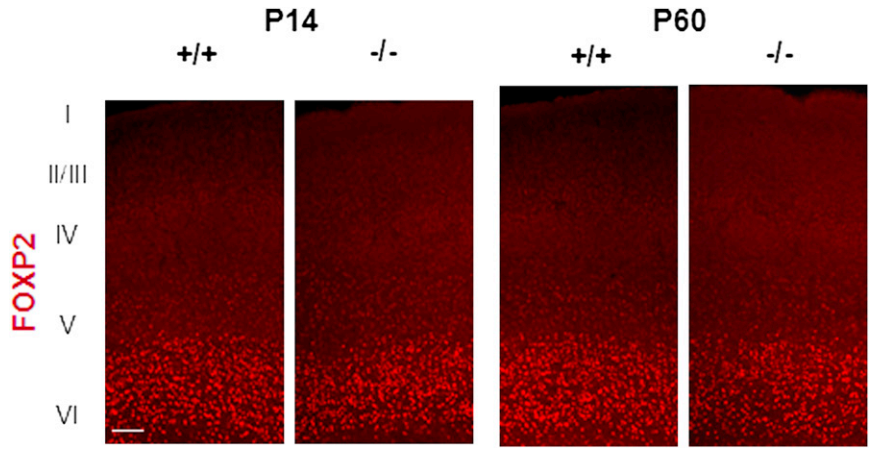

Figure S2. Normal Distribution of Early Born Cortical Neurons in *Cntnap2*$^{-/-}$ Mice, Related to Figure 2

Expression of *Foxp2*, a marker for deep layer projection neurons in somatosensory cortex of WT and *Cntnap2* KO mice. n = 3 mice/genotype for each age. Scale bar: 50 μm.

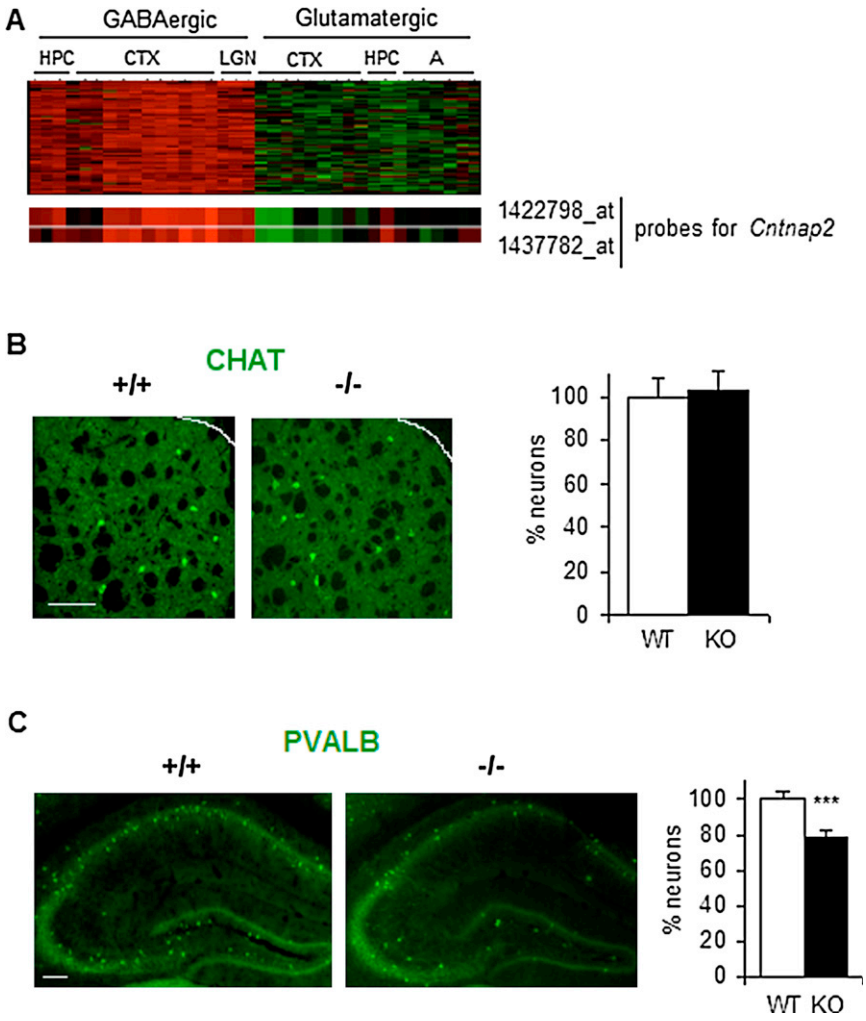

Figure S3. Interneurons in *Cntnap2*$^{-/-}$ Mice, Related to Figure 1 and Figure 3

(A) Heatmap showing the expression level (red: high, green: low) of the genes within the *Cntnap2* module. Genes are represented in rows and neuronal populations in columns. CTX, cortex; HPC, hippocampus; LGN, lateral geniculate nucleus; A, amygdala.

(B) Expression of *Chat*, a marker for cholinergic interneurons in striatum of WT and *Cntnap2* KO mice at P14. Scale bar: 100 μm.

(C) PVALB interneurons in adult hippocampus. Scale bar: 100 μm.

For (B) and (C) n = 3 mice/genotype. Data are presented as mean ± SEM. ***$p < 0.001$.

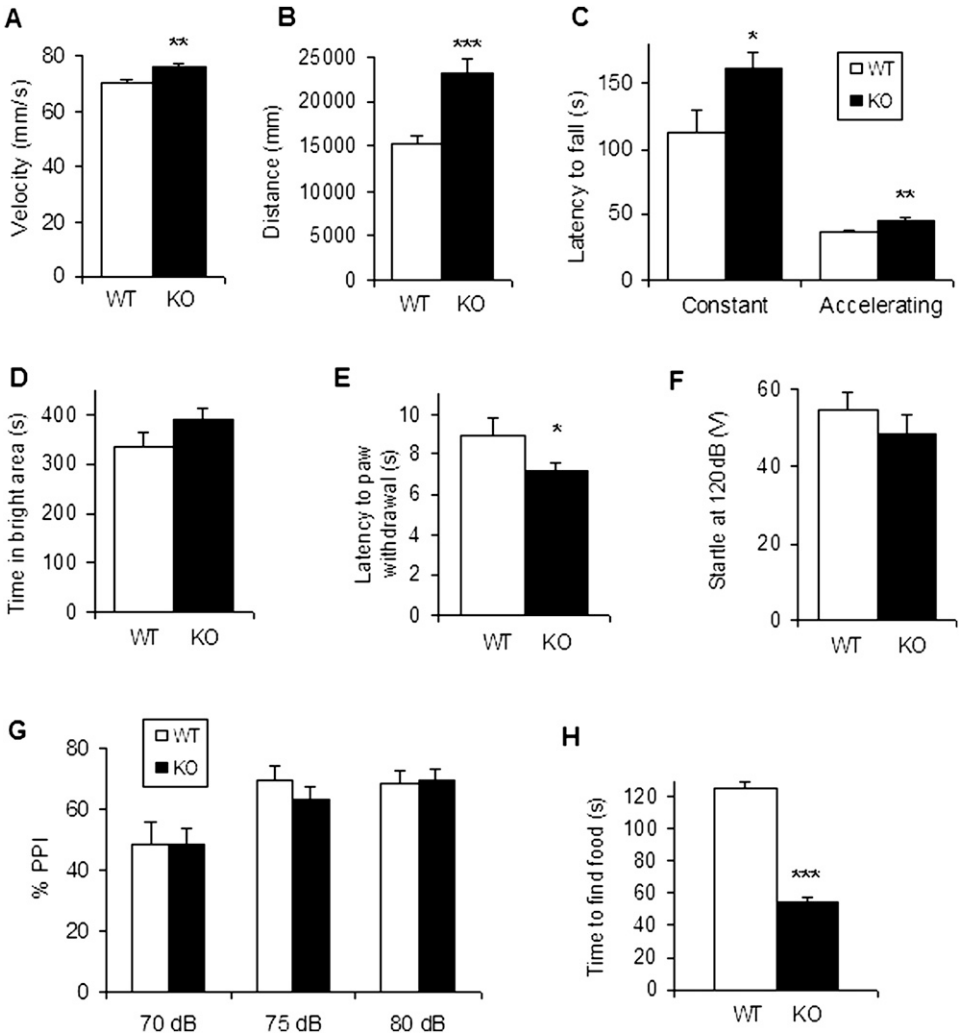

Figure S4. *Cntnap2*$^{-/-}$ Mice Show Hyperactivity and Hyperreactivity to Sensory Stimuli, Related to Figure 5

(A and B) Open field test. Distance traveled (A) and velocity (B) during the 20 min test.

(C) Rotorod. Latency to fall from the rotorod (up to 180 s) in the constant and accelerating speed tasks.

(D) Light-dark box test. Data show the time spent in the bright area during the 10 min test.

(E) Hot plate test. Latency to paw withdrawal from a plate at 52.5°C (up to 15 s).

(F and G) Startle response and prepulse inhibition. (F) Startle amplitude upon a 120 dB sound and (G) percentage of inhibition of the original startle when receiving 70 dB, 75 dB and 80 dB sounds prior to the 120 dB startling sound.

(H) Olfaction test. Time to find buried food. Data are presented as mean ± SEM.*$p < 0.05$, **$p < 0.01$, ***$p < 0.001$.

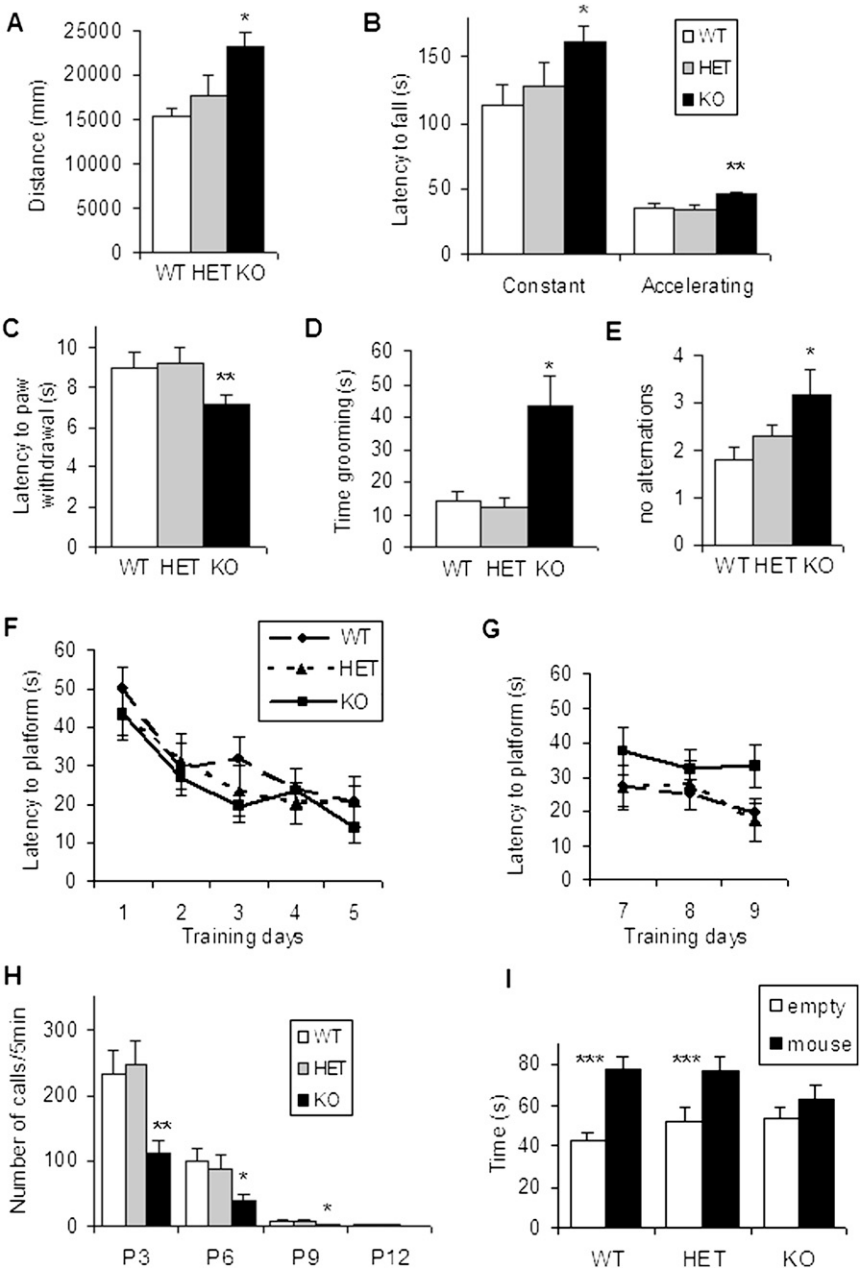

Figure S5. No Behavioral Abnormalities Are Seen in *Cntnap2* $^{+/-}$ Mice, Related to Figure 5 and Figure 6

(A) Open field test showing the distance traveled during the 20 min test.

(B) Rotorod. Latency to fall from the rotorod (up to 180 s) in the constant and accelerating speed tasks.

(C) Hot plate test. Latency to paw withdrawal from a plate at 52.5°C (up to 15 s).

(D) Time spent grooming in 10 min.

(E) Number of no alternations in the T maze spontaneous alternation test.

(F and G) Morris water maze test. Learning curves for the learning (F) and reverse learning (G) tasks of the test.

(H) Ultrasonic vocalizations in pups separated from the dam.

(I) Three chamber social interaction test. Time spent sniffing an inanimate object (empty cup) versus a cup with a mouse is presented. Data are presented as mean ± SEM.*p < 0.05, **p < 0.01, ***p < 0.001.